Available online at www.sciencedirect.com
ScienceDirect
Trans. Nonferrous Met. Soc. China 33(2023) 59−66
Transactions of Nonferrous Metals Society of China
www.tnmsc.cn

Effect of ultrasonic vibration on microstructure and mechanical properties of $Mg_{98}Y_{1.0}Ni_{0.5}Al_{0.5}$ alloy containing LPSO structure

Shu-lin LÜ[1], Di-jia ZHAO[1], Xiao-yuan JI[1], Wei GUO[1,2,3]

1. State Key Lab of Materials Processing and Die & Mould Technology,
School of Materials Science and Engineering, Huazhong University of Science and Technology, Wuhan 430074, China;
2. State Key Laboratory of Advanced Design and Manufacturing for Vehicle Body,
Hunan University, Changsha 410082, China;
3. Research Institute of Huazhong University of Science and Technology in Shenzhen, Shenzhen 518057, China

Received 30 September 2021; accepted 28 February 2022

Abstract: The LPSO structure reinforced magnesium alloy with low Y and Ni contents can achieve the best balance between performance and cost. To further improve the comprehensive mechanical properties, doping with Al element and ultrasonic vibration treatment are feasible approaches. The microstructure of low Y and Ni containing $Mg_{98}Y_{1.0}Ni_{0.5}Al_{0.5}$ alloy with Al addition and the effect of ultrasonic vibration on the microstructure and mechanical properties were studied by SEM−EDS, TEM, XRD and nano-indentation. Doping Al into the alloy decreases the amount of LPSO structure, and Al_2NiY phases with radial morphology precipitate near the block LPSO structure. The Al_2NiY phase is non-coherent with LPSO structure and Mg matrix at the phase interfaces. The Al_2NiY phase can be effectively modified into short flakes and distributed uniformly in the matrix with ultrasonic vibration treatment. The mechanical properties of $Mg_{98}Y_{1.0}Ni_{0.5}Al_{0.5}$ alloy are improved by reducing the generation of microcracks and preventing their propagation. Compared with $Mg_{98}Ni_{0.5}Y_{1.0}Al_{0.5}$ alloy without ultrasonic vibration treatment, the ultimate tensile strength and elongation of the alloy with ultrasonic vibration treatment are improved to 187 MPa and 7.9%, with increments of 21.4% and 105.7%, respectively.

Key words: Mg−Y−Ni−Al alloy; LPSO structure; ultrasonic vibration; microstructure; mechanical properties

1 Introduction

Long period stacking ordered (LPSO) structure reinforced magnesium alloys exhibit excellent mechanical properties and have received favorable attentions in recent years [1−3]. The LPSO-containing Mg−Y−Ni system is a promising magnesium alloy with excellent strength [4]. Some research has revealed that the strength of alloys is proportional to the volume fraction of LPSO. The extruded Mg−20.1Y−13.3Ni (wt.%) alloy with high volume fraction of LPSO structure possesses a compressive yielding strength of 602 MPa, an ultimate compressive strength of 763 MPa and an elongation to failure of 7.8% at RT [5]. Even though the high volume fraction of LPSO structure can strengthen magnesium alloys significantly, the high contents of Y and Ni increase the cost of this alloy [6,7]. Therefore, addition of some inexpensive alloying elements in Mg alloys to participate in the formation of LPSO structure or precipitate new strengthening phases is necessary.

TAN et al [8] studied the microstructure and mechanical properties of $Mg_{97.76}Y_{1.06}Zn_{0.76}Al_{0.42}$ (at.%) subjected to annealing and extrusion. The

Corresponding author: Wei GUO, Tel: +86-27-87556262, E-mail: weiguo@hust.edu.cn;
Xiao-yuan JI, Tel: +86-27-87541922, E-mail: jixiaoyuan@hust.edu.cn
DOI: 10.1016/S1003-6326(22)66090-4

Mg_4Y_2ZnAl phase could complement the LPSO in contributing to the strength of the alloy through second phase hardening. KISHIDA et al [9] found that the Al and Gd atoms could gather to form Al_6Gd_8 cluster structure in Mg−Al−Gd alloy and transformed into a long-range ordered structure which differed from the general LPSO structure. Furthermore, DAI et al [10] doped Al into Mg−Gd−Y alloy and found that α-Mg grains were refined significantly and the properties of the alloy were increased. Therefore, Al should be a promising alternative to improve the overall performance of LPSO-containing Mg alloy.

The properties of alloys depend not only on the volume fraction of strengthening phases, but also on the morphology and size of these phases. Ultrasonic vibration (UV) treatment is an effective and convenient method to refine and modify the second phases such as LPSO structure and Mg_2Si in Mg alloys, thereby enhancing the properties of alloys [11]. Thus, in the present study, the microstructure and performance of an LPSO-formable and low Ni and Y containing Mg−Y−Ni−Al alloy with UV treatment were investigated in detail.

2 Experimental

In this study, the pure Mg (99.95 wt.%), Ni (99.9 wt.%), Al (99.95 wt.%) and Mg−30wt.%Y alloy were used as the raw materials to prepare $Mg_{98}Y_{1.0}Ni_{0.5}Al_{0.5}$ (at.%) alloy. The raw materials were melted at 780 °C in a resistance furnace under an atmosphere of 0.1 vol.% SF_6 and 99.9 vol.% N_2. The melted alloy without UV treatment (named as WNA100 alloy) was de-gassed with high-purity Ar gas at 730 °C and then poured into a mold preheated to 200 °C. The alloy with ultrasonic vibration treatment (named as WNA100-UV alloy) was prepared by the equipment shown in Fig. 1. The molten alloy after de-gassing was placed in the holding furnace and then the ultrasonic horn was inserted into the molten alloy at 655−660 °C. The power of UV was 1800 W and the processing duration was 60−80 s. After that, the molten alloy was poured into the mold. The size of the casting was 30 mm in diameter and 100 mm in length.

A small specimen was cut from the upper center of the as-cast sample. After grinding, polishing, and etching, microstructures of the samples were observed with a Nova Nano SEM 450 equipped with an EDS detector and a Tecnai G2−F30 TEM. Phase compositions were detected with an Empyrean XRD at a scanning speed of 15 (°)/min from 10° to 90°. For TEM observation, the specimens were processed to 50 μm in thickness and 3 mm in diameter firstly. Then, they were thinned by twin jet electropolishing at parameters of 70 V, −20 °C. The nano-indentation testing was conducted by Hysitron TI 750 nanoindentor with a load of 2 mN and 20 indents were tested on each phase. The strength and elongation of the alloys were tested by a SHIMADZU AG IC−100 kN material testing machine at a tensile speed of 1 mm/min. The sketch of tensile test sample is shown in Fig. 2.

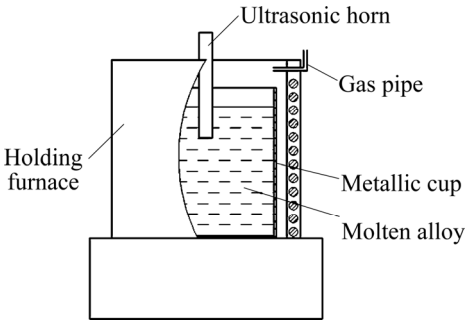

Fig. 1 Schematic of ultrasonic equipment

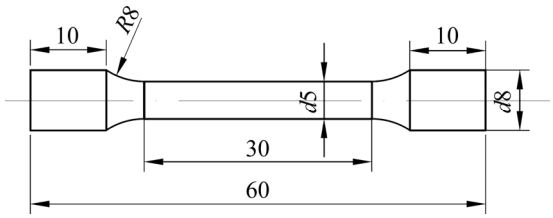

Fig. 2 Sketch of tensile test sample (Unit: mm)

3 Results and discussion

3.1 Microstructures of WNA100 and WNA100-UV alloys

Figure 3 shows the phase analysis results of WNA100 and WNA100-UV alloys by XRD. According to the previous study, $Mg_{98.5}Y_{1.0}Ni_{0.5}$ alloy without UV treatment (named as WN10 alloy) consists of α-Mg and LPSO structure [11]. In WNA100 alloy, the crystalline peaks from Al_2NiY phase can be also detected besides α-Mg and LPSO structure. Furthermore, the intensity of the diffraction peaks from Al_2NiY phase and LPSO structure in WNA100-UV is stronger, compared with that in WNA100.

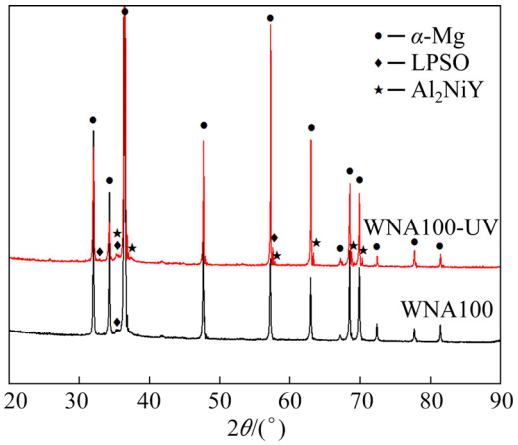

Fig. 3 XRD patterns of WNA100 and WNA100-UV alloys

Figure 4 shows the microstructures of WNA100 and WNA100-UV alloys observed with SEM. According to previous research, the microstructure of WN10 alloy consists of dendrite α-Mg grains and network LPSO structure distributed along the grain boundary [12]. After doping with 0.5 at.% Al (Figs. 4(a, b)), the gray LPSO structure and a new bright and flaky phase can be observed at the grain boundary in the WNA100 alloy. The volume fraction of gray LPSO structure decreases obviously compared with that in the previous study on WN10 [13]. After UV treatment (Figs. 4(c, d)), the secondary phases are distributed more uniformly compared with those counterparts without UV. The volume fractions of both gray LPSO structure and bright phase increase, compared with those in WNA100. Most importantly, most flaky phase with large size disappears and its branches are broken into short flakes.

To figure out the composition of the phases with various morphologies, the EDS analysis was conducted. The EDS results in Table 1 show that the composition of the block bright phase in WNA100 from Fig. 4(b) is Mg−12.71at.%Y−10.5at.%Ni−24.69at.%Al. The Al content in the bright phase suggests that Al participates in the formation of this bright phase. The composition of short plate phase in WNA100-UV from Fig. 4(d) is Mg−4.29at.%Ni−5.44at.%Y−11.80at.%Al. The molar ratio between Y, Ni and Al of bright phase in both WNA-100 and WNA100-UV alloys is very close to 1:1:2. Thus, the block bright phase in WNA100 and the large or fine flaky phase in WNA100-UV are considered to be Al_2NiY phase. By comparing the distribution of Al_2NiY in WNA100 and WNA100-UV, it is noted that the

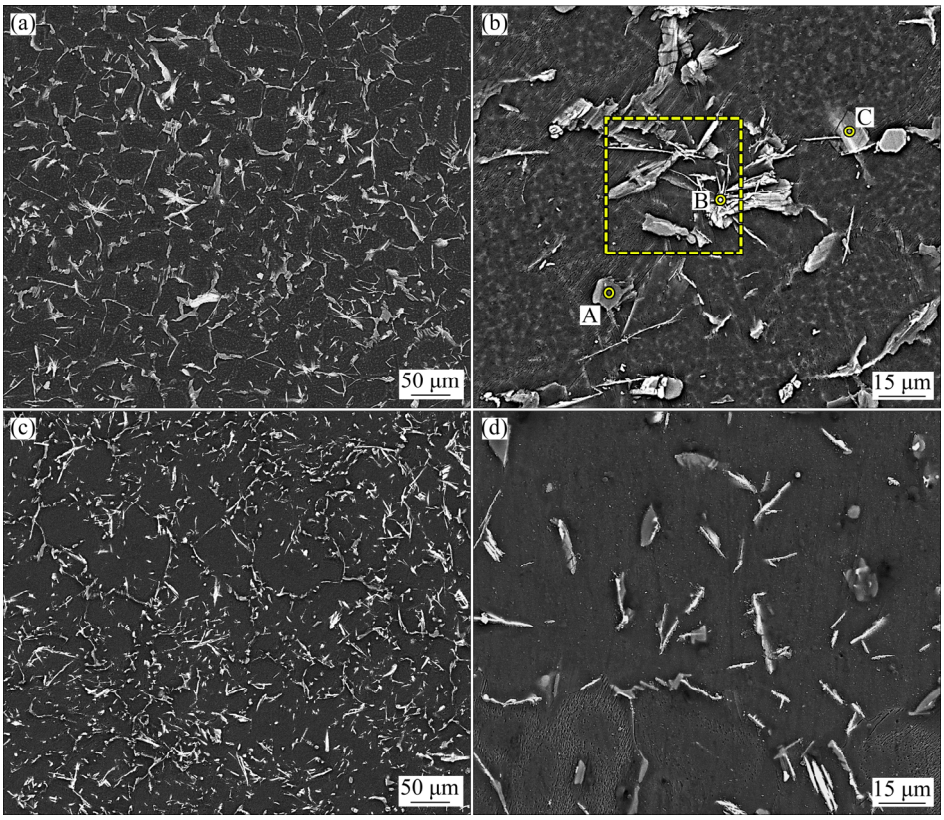

Fig. 4 Microstructures of $Mg_{98}Ni_{0.5}Y_{1.0}Al_{0.5}$ alloy under SEM/BSE: (a, b) WNA100; (c, d) WNA100-UV

Table 1 Compositions of secondary bright phases in WNA100 alloy with different morphologies in Fig. 4(b)

Phase	Y	Ni	Al	Mg
A	3.89	3.48	−	Bal.
B	12.71	10.5	24.69	Bal.
C	6.53	5.98	12.95	Bal.

application of UV contributes to obvious refinement and uniform distribution of the Al_2NiY phase. This phenomenon can be ascribed to the acoustic streaming effect induced by UV treatment. During UV treatment, ultrasound is produced and propagates throughout the melt. The convection of the molten alloy is intensified, and a cyclic acoustic streaming appears in the fluid [13,14]. The solute atoms (Al, Ni and Y) are distributed more uniformly via the acoustic streaming. Solute segregation in the diffusion layer can be alleviated or removed. Then, the Al_2NiY phase has nearly the same undercooling and growth velocity in all directions at the solidification front, so that the growth of the grain is restricted.

Figure 5(a) shows the microstructure of WNA100 alloy observed with TEM. The large white area is the Mg grains. The secondary phases include the gray and black phases. Figure 5(b) shows the high-resolution image of the gray phase, revealing black streaks with constant spacing. The black layers are enriched with Ni and Y atoms while the bright layers are the magnesium matrix. The periodical stacking of Ni−Y atoms in the matrix contributes to the formation of LPSO structure. The corresponding selected area electron diffraction (SAED) is shown in Fig. 5(c). Five representative additional spots between two highlight spots can be observed, which indicates a 18R-type LPSO structure [15,16]. These results suggest that the type of LPSO structure cannot be changed by doping Al, even though some secondary phase precipitates near them. Figures 5(d, e) show the high-resolution image and SAED result of black phase, respectively. The lattice fringe exhibits large difference from LPSO structure, with a lattice fringe spacing of 0.258 nm. The calibrated result confirms that the black phase is Al_2NiY phase.

Figure 6 shows various morphologies of Al_2NiY phase in WNA100-UV observed with TEM. As shown in Fig. 6(a), the small Al_2NiY phase is completely surrounded by LPSO structure. Figure 6(c) shows the high-resolution image of the interface between LPSO structure and Al_2NiY phase, as well as the corresponding fast Fourier transform (FFT) results. It is noted that the $(02\bar{1})_{Al_2NiY}$ is not exactly parallel to $(0018)_{LPSO}$, with an angle of about 3.22°, indicating that these two phases are not coherent at their interface. Figure 6(b) shows a single Al_2NiY crystal with larger size. The Al_2NiY connects with the matrix but no LPSO structure can be observed around it. The FFT result at the Al_2NiY/α-Mg interface exhibits that there is no orientation relation between these two phases, indicating the non-coherent relation.

The main reason for the various morphologies of Al_2NiY phase is the heterogeneous distribution of Al atoms. If Al atoms are sufficient, the Al_2NiY phase will grow into large size and no redundant Ni

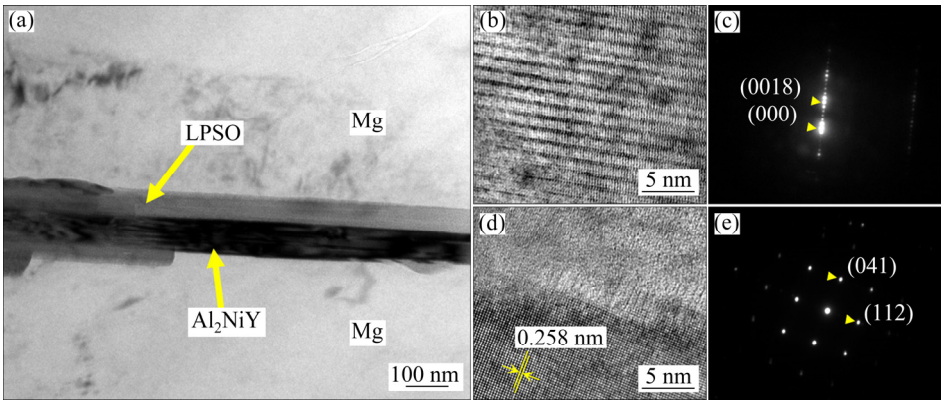

Fig. 5 Results of TEM observation in WNA100: (a) Bright-field image showing two kinds of phases with different contrasts; (b) High-resolution image of gray phase; (c) SAED result of gray phase with electron beam parallel to $\langle 11\bar{2}0\rangle$; (d) High-resolution image of black phase; (e) SAED results of black phase with electron beam parallel to $\langle 71\bar{4}\rangle$

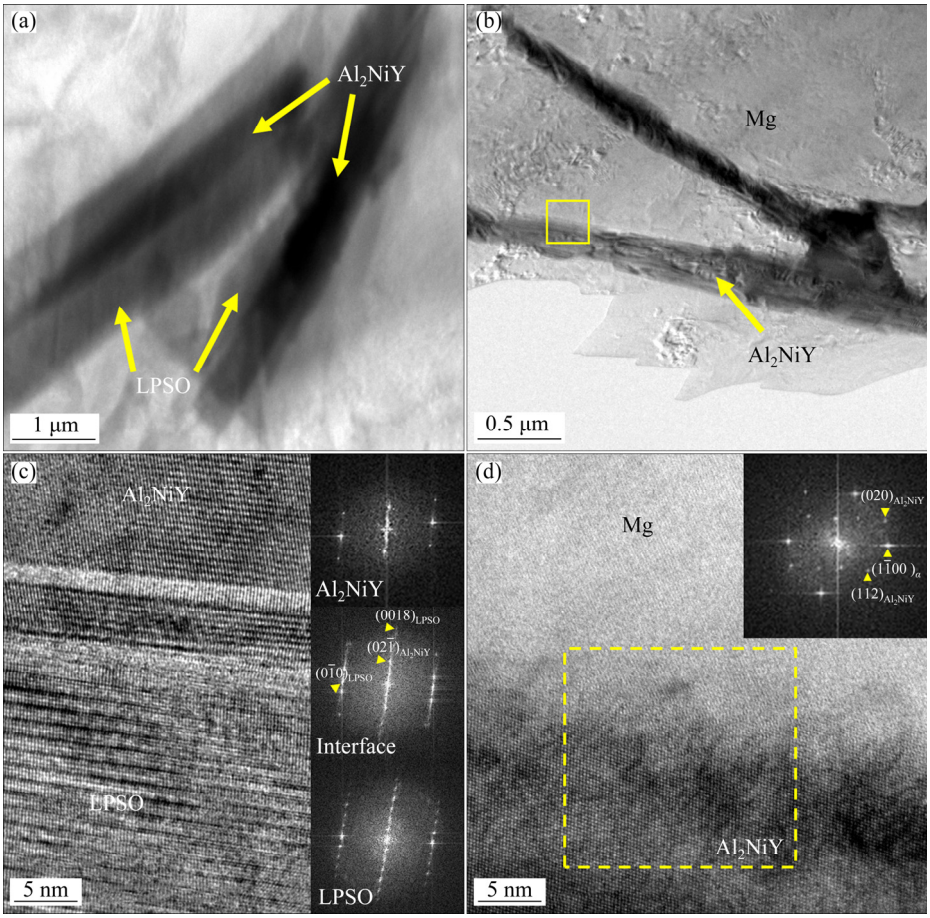

Fig. 6 Morphologies of Al_2NiY phase observed with TEM in WNA100-UV: (a, b) Bright-field images; (c) High-resolution image taken at interface between Al_2NiY phase and LPSO structure and corresponding FFT results; (d) High-resolution image taken at interface between Al_2NiY phase and Mg matrix and corresponding FFT results

and Y atoms participate in the formation of LPSO structure. Thus, LPSO structure cannot be found near Al_2NiY phase (as shown in Fig. 6(b)). If Al atoms are lacking, the remanding Ni and Y atoms contribute to the formation of LPSO structure, and thus, LPSO structure is distributed around Al_2NiY phase (as shown in Fig. 6(a)).

The formation of Al_2NiY phase after doping Al demonstrates that the precipitation of Al_2NiY is easier than that of LPSO structure. During solidification process, the solute atoms are pushed forward with the growth of α-Mg grains. During the formation of LPSO structure, large amount of stacking faults are formed in the matrix and Ni−Y atomic clusters are formed. Then, these Ni−Y atomic clusters stack orderly with a specific period, contributing to the formation of LPSO structure. The doped Al may affect the above process. The electronegativity difference between Al (1.61) and Y (1.22) is larger than that between Mg (1.31) and Y (1.22), which leads to a stronger affinity of Al−Y. Therefore, Y atoms tend to participate in the formation of Al_2NiY phase. With less Y in the matrix, the amount of stacking faults decreases and the formation of LPSO structure is restrained. After Al atoms are consumed completely, the residual Ni−Y atoms participate in the formation of LPSO structure.

3.2 Mechanical properties of WNA100 and WNA100-UV alloys

Figure 7 shows the mechanical properties of $Mg_{98}Ni_{0.5}Y_{1.0}Al_{0.5}$ alloy without and with UV. The ultimate tensile strength (UTS) and elongation (EL) of WNA100 alloy are 154 MPa and 3.84%, respectively. The UTS and EL of WNA100-UV alloy reach 187 MPa and 7.9%, which are enhanced by 21.4% and 105.7% compared with WNA100 alloy, respectively.

According to the previous researches, the 18R-type LPSO structure is coherent with α-Mg at the interface, leading to a high bonding strength

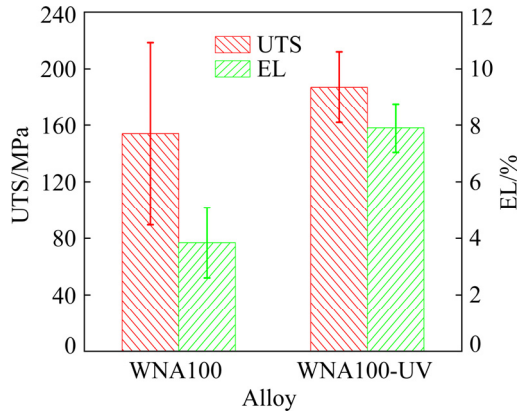

Fig. 7 Mechanical properties of WNA100 and WNA100-UV alloys

of the interface [17−19]. In addition, the LPSO structure has good deformability [20−22]. Thus, both UTS and elongation can be improved by precipitated LPSO structure. Therefore, the refined and homogenized LPSO structure in WNA100-UV should contribute to the improved mechanical properties.

The effects of the newly-precipitated Al_2NiY phase on the mechanical properties have also been studied. Figure 8 shows the longitudinal sections of the tensile fracture surface of WNA100 and WNA100-UV alloys. Microcracks can be observed around Al_2NiY phase in WNA100 alloy. The initiation of these microcracks may result from the different properties of various phases (α-Mg matrix, LPSO and Al_2NiY). To discuss these differences among various phases, a nano-indentation test has been performed. The load-depth curves are shown in Fig. 9. The hardness (H) is given by Eq. (1) based on the Oliver–Pharr method [23]:

$$H=P_{max}/A \quad (1)$$

where P_{max} is the peak load and A is the projected area of indentation. The average hardness of the matrix, LPSO and Al_2NiY are (1.41±0.23), (2.02±0.251) and (2.45±0.34) GPa, respectively. The different hardness values results in different deformabilities. During tensile testing, they deform discriminately, and high stress concentration should occur at the interface. Furthermore, the interfaces of Al_2NiY/matrix and Al_2NiY/LPSO have been confirmed as non-coherent interface, which suggests a weak bonding strength. Thus, the interfaces can be departed easily and microcracks initiate. Consequently, alloys containing Al_2NiY show a premature fracture and the strengthening effect originated from LPSO structure is inhibited.

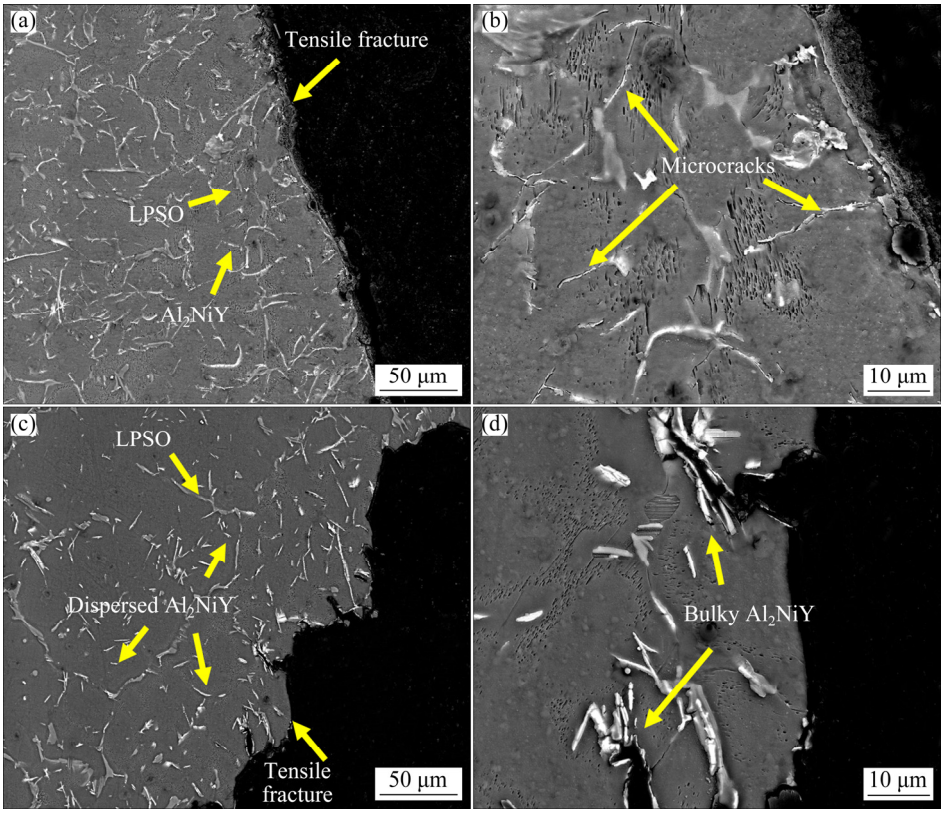

Fig. 8 Morphologies for longitudinal sections of tensile fracture: (a, b) WNA100; (c, d) WNA100-UV

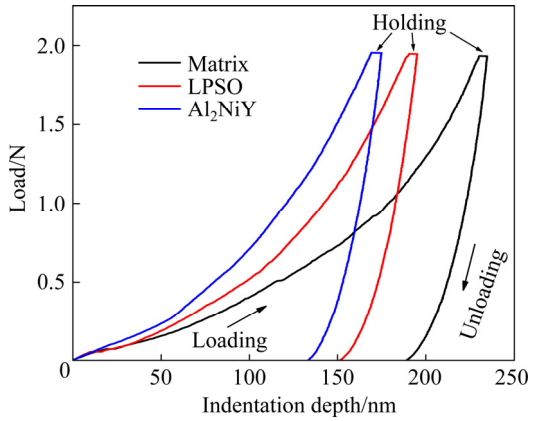

Fig. 9 Nano-indentation testing results of α-Mg matrix, LPSO and Al_2NiY phases

Most radially block Al_2NiY phase are modified to short flakes and distributed more uniformly in WNA100-UV. As shown in Figs. 8(c, d), the cracks resulted from few un-refined Al_2NiY phase is the main reason for the fracture. No microcrack is found around the fine and homogenized Al_2NiY phase. During deformation, dislocations are easier to steer by the refined Al_2NiY phase than by radial morphology. Thus, the matrix around them can undergo a larger amount of deformation before the crack initiation at Al_2NiY/α-Mg interface. Moreover, the randomly distributed Al_2NiY phase is helpful to hinder the propagation of the cracks initiating at the boundary of Al_2NiY phase. Then, the large cracks are difficult to propagate, and the fracture is delayed. As a result, the mechanical properties of WNA100 alloy can be improved by UV treatment.

4 Conclusions

(1) In the LPSO-containing Mg−Y−Ni−Al alloy, Al element cannot participate in the formation of LPSO structure, and it inhibits the growth of LPSO structure by consuming Ni and Y elements to form Al_2NiY phase.

(2) The Al_2NiY phase with radial morphology is not coherent with the LPSO structure and α-Mg matrix at the interfaces. This radial Al_2NiY phase can be effectively modified into short flakes and distributed more uniformly in the matrix by UV treatment.

(3) The initiation of microcracks in WNA100 alloy is resulted from different properties of α-Mg matrix, LPSO structure and Al_2NiY phase. The refined Al_2NiY phase in WNA100-UV alloy can reduce the generation and propagation of microcracks. The large cracks are difficult to initiate, and the fracture is delayed.

(4) After UV treatment, the UTS and elongation reach 187 MPa and 7.9%, which are enhanced by 21.4% and 105.7%, respectively, compared with those of the alloy without UV.

Acknowledgments

The authors are grateful for the financial supports from the National Natural Science Foundation of China (Nos. 52175321, 52101138), Start-up Fund from Huazhong University of Science and Technology, China (Nos. 3004110125, 3004110142), State Key Lab of Advanced Metals and Materials, China (No. 2020-Z01), State Key Laboratory for Mechanical Behavior of Materials, China (No. 20202205), State Key Laboratory of Advanced Design and Manufacturing for Vehicle Body, China (No. 32015001), Guangdong Basic and Applied Basic Research Foundation, China (No. 2020A1515110531), and Natural Science Foundation of Hubei Province, China (No. 2020CFB259).

References

[1] KISHIDA K, NAGAI K, MATSUMOTO A, YASUHARA A, INUI H. Crystal structures of highly-ordered long-period stacking-ordered phases with 18R, 14H and 10H-type stacking sequences in the Mg−Zn−Y system [J]. Acta Materialia, 2015, 99: 228−239.

[2] TANG P Y, WU M J, TANG B Y, WANG J W, PENG L M, DING W J. Microstructure of 18R-type long period ordered structure phase in $Mg_{97}Y_2Zn_1$ alloy [J]. Transactions of Nonferrous Metals Society of China, 2011, 21(4): 801−806.

[3] DING Z B, ZHAO Y H, LU R P, YUAN M N, WANG Z J, LI H J, HOU H. Effect of Zn addition on microstructure and mechanical properties of cast Mg−Gd−Y−Zr alloys [J]. Transactions of Nonferrous Metals Society of China, 2019, 29(4): 722−734.

[4] GUO Y L, LUO Q, LIU B, LI Q. Elastic properties of long-period stacking ordered phases in Mg−Zn−Y and Mg−Ni−Y alloys: A first-principles study [J]. Scripta Materialia, 2020, 178: 422−427.

[5] ZHU S M, LAPOVOK R, NIE J F, ESTRIN Y, MATHAUDHU S N. Microstructure and mechanical properties of LPSO phase dominant Mg85.8Y7.1Zn7.1 and Mg85.8Y7.1Ni7.1 alloys [J]. Materials Science and Engineering A, 2017, 692: 35−42.

[6] WANG J F, GAO S Q, LIU X Y, PENG X, WANG K, LIU S J, JIANG W Y, GUO S F, PAN F S. Enhanced mechanical properties and degradation rate of Mg−Ni−Y alloy by introducing LPSO phase for degradable fracturing ball applications [J]. Journal of Magnesium and Alloys, 2020, 8(1):127−133.

[7] WU S Z, QIAO X G, ZHENG M Y. Ultrahigh strength Mg−Y−Ni alloys obtained by regulating second phases [J]. Journal of Materials Science & Technology, 2020, 45: 117−124.
[8] TAN X, CHEE K H W, CHAN K W J, RICHARD K W O, GUPTA M. Effect of homogenization on enhancing the failure strain of high strength quaternary LPSO Mg−Y−Zn−Al alloy [J]. Materials Science and Engineering A, 2015, 644: 405−412.
[9] KISHIDA K, YOKOBAYASHI H, INUI H, YAMASAKI M, KAWAMURA Y. The crystal structure of the LPSO phase of the 14H-type in the Mg−Al−Gd alloy system [J]. Intermetallics, 2012, 31: 55−64.
[10] DAI J, ZHU S, EASTON M A, ZHANG M, QIU D, WU G, LIU W, DING W. Heat treatment, microstructure and mechanical properties of a Mg−Gd−Y alloy grain-refined by Al additions [J]. Materials Science and Engineering A, 2013, 576: 298−305.
[11] YANG X, WU S S, LÜ S L, HAO L Y, FANG X G. Refinement of LPSO structure in Mg−Ni−Y alloys by ultrasonic treatment [J]. Ultrasonics Sonochemistry, 2018, 40: 472−479.
[12] YANG X, WU S S, LÜ S L, HAO L Y, FANG X G. Effects of Ni levels on microstructure and mechanical properties of Mg−Ni−Y alloy reinforced with LPSO structure [J]. Journal of Alloys and Compounds, 2017, 726: 276−283.
[13] XUE H S, XING Z H, ZHANG W N, YANG G, PAN F S. Effects of ultrasonic treatment on microstructure and mechanical properties of Mg−6Zn−0.5Y−2Sn alloy [J]. Transactions of Nonferrous Metals Society of China, 2016, 26(7): 1826−1834.
[14] YANG Y S, WANG J C, WANG T, LIU C M, ZHANG Z M. Effects of ultrasonic treatment on microstructures of AZ91 alloy [J]. Transactions of Nonferrous Metals Society of China, 2014, 24(1): 76−81.
[15] ZHU Y M, MORTON A J, NIE J F. The 18R and 14H long-period stacking ordered structures in Mg−Y−Zn alloys [J]. Acta Materialia, 2010, 58: 2936−2947.
[16] ZHU Y M, MORTON A J, NIE J F. Growth and transformation mechanisms of 18R and 14H in Mg−Y−Zn alloys [J]. Acta Materialia, 2012, 60: 6562−6572.
[17] HAGIHARA K, KINOSHITA A, SUGINO Y, YAMASAKI M, KAWAMURA Y, YASUDA H Y, UMAKOSHI Y. Effect of long-period stacking ordered phase on mechanical properties of Mg97Zn1Y2 extruded alloy [J]. Acta Materialia, 2010, 58: 6282−6293.
[18] SHAO X H, YANG Z Q, MA X L. Strengthening and toughening mechanisms in Mg−Zn−Y alloy with a long period stacking ordered structure [J]. Acta Materialia, 2010, 58: 4760−4771.
[19] HAGIHARA K, YOKOTANI N, UMAKOSHI Y. Plastic deformation behavior of Mg12YZn with 18R long-period stacking ordered structure [J]. Intermetallics, 2010, 18: 267−276.
[20] KAWAMURA Y, KASAHARA T, IZUMI S, YAMASAKI M. Elevated temperature Mg97Y2Cu1 alloy with long period ordered structure [J]. Scripta Materialia, 2006, 55: 453−456.
[21] LIU H, XUE F, BAI J, ZHOU J, SUN Y S. Microstructure and mechanical properties of Mg94Zn2Y4 extruded alloy with long-period stacking ordered structure [J]. Transactions of Nonferrous Metals Society of China, 2013, 23(12): 3598−3603.
[22] LU F M, MA A B, JIANG J H, YANG D H, YUAN Y C, ZHANG L Y. Formation of profuse long period stacking ordered microcells in Mg−Gd−Zn−Zr alloy during multipass ECAP process [J]. Journal of Alloys and Compounds, 2014, 601: 140−145.
[23] OLIVER W C, PHARR G M. An improved technique for determining hardness and elastic modulus using load and displacement sensing indentation experiments [J]. Journal of Materials Research, 1992, 7(6): 1564−1583.

超声振动对含 LPSO 结构的 $Mg_{98}Y_{1.0}Ni_{0.5}Al_{0.5}$ 合金显微组织与力学性能的影响

吕书林[1]，赵第甲[1]，计效园[1]，郭 威[1,2,3]

1. 华中科技大学 材料科学与工程学院 材料成型与模具国家重点实验室，武汉 430074；
2. 湖南大学 汽车车身先进设计制造国家重点实验室，长沙 410082；
3. 深圳华中科技大学研究院，深圳 518057

摘 要：低 Y、Ni 含量的 LPSO 结构增强镁合金具有低成本、优异力学性能的特点。为进一步提升其综合力学性能，掺杂 Al 元素及熔体超声振动处理是可行的途径。通过扫描电子显微镜、能谱分析、透射电子显微镜、X 射线衍射和纳米压痕测试研究掺杂 Al 元素后低 Y、Ni 含量的 $Mg_{98}Y_{1.0}Ni_{0.5}Al_{0.5}$ 合金的显微组织，对比超声振动对显微组织与力学性能的影响。掺杂 Al 后 LPSO 结构的含量降低，且在块状 LPSO 结构相邻处析出圆整的 Al_2NiY 相。Al_2NiY 相与 LPSO 结构和 Mg 基体在界面处均不共格。通过对熔体施加超声振动处理后，Al_2NiY 相被有效细化为短片状，并均匀分布在基体中，阻碍微裂纹的产生和扩展，从而提高 $Mg_{98}Ni_{0.5}Y_{1.0}Al_{0.5}$ 合金的力学性能。与未经超声处理 $Mg_{98}Ni_{0.5}Y_{1.0}Al_{0.5}$ 合金相比，其极限抗拉强度和伸长率提升至 187 MPa 和 7.9%，分别增长 21.4% 和 105.7%。

关键词：Mg−Y−Ni−Al 合金；LPSO 结构；超声振动；显微组织；力学性能

(Edited by Bing YANG)